Sensors-25539-2019

Sensing performance of Nanocrystalline Graphite Based Humidity Sensors

Ting Yang Ling, *Member, IEEE,* Suan Hui Pu, *Member, IEEE,* Sam J. Fishlock, Yisong Han, Jamie D Reynolds, John W. McBride, Harold M.H. Chong, *Member, IEEE*

***Abstract*— Environmental sensors play a crucial role in a wide range of applications. Amongst them, humidity sensors that are stable and operational in harsh environments are incredibly important for process control and monitoring. Nanocrystalline graphite (NCG) is a type of carbon-based thin film material. Previous work has shown that NCG has excellent mechanical properties and is able to withstand high radiation doses. The granular structure of the NCG film makes it a good candidate for humidity sensing as the film consists of conductive graphitic grains with a high density of sp^2 bonds and amorphous grain boundaries with high resistivity, adsorption of water molecule onto the film forms conductive pathways between grains through the Grotthuss mechanism which lowers the resistance of the film by a measurable amount. Here we report for the first time, a working humidity sensor with linear response, fabricated using NCG as the sensing material for harsh, real-world environments, which include exposure to weak acids via rainfall, UV radiation, mechanical wear, and high humidity environments. The calculated sensitivity of the best-fabricated sensor is S = 0.0334%, with a maximum resistance change of -4.4 kOhms, over the range of 15% RH to 85% RH. The response time of the sensor is 20ms with the current measurement setup. The baseline resistance value of the sensor at 15% RH is 210 kOhms. The sensor has the potential to be used as a humidity sensor for harsh environments due to the chemical, thermal and mechanical stability of the NCG film.**

***Index Terms*—**Nanocrystalline Graphite, PECVD, Humidity Sensors, Harsh environment

I. INTRODUCTION

TO PREDICT, analyze and optimize our lifestyle and environmental impacts, a vast amount of data is needed. These data could be obtained via ubiquitous sensors, implanted in everyday objects. For this to be realized, small, low-powered sensing devices are ideal. Amongst environmental metrics, humidity is one of the most important. It can be used to predict weather patterns [1], maintain workplace comfort [2], [3], preserving sensitive artifacts [4], and maintaining product quality in the manufacturing industry [5]. Ceramic-based sensors are often used for resistive humidity sensing applications [6], [7], etc. These sensors work by protonic conduction, where the water vapour is adsorbed onto the surface of porous ceramic materials. Due to the Grotthuss mechanism, where charge is conducted by the adsorbed water via proton hopping, and thus, changing the measured resistance of the films. Metal oxide thin film sensors are also widely used for manufacturing various gas and humidity sensors [8], [9]. However, ceramic and metal oxide films require higher operating temperatures, and thus, may not be suitable for some applications. Polymer-based humidity sensors, such as polyimide, pentacene, conductive polymers such as polypyrrole and polyaniline, which have lower operating temperatures have also been proposed [10]–[12]. These sensors work by measuring the mechanical (gravimetric, geometrical) or electrical change (capacitance, resistance) of the polymer film due to moisture absorption. For gravimetric and geometrical measurements, it is often difficult to distinguish between the mass-shift and film expansion due to absorption by other vapour and water. Furthermore, polymer films are known to suffer from photo-induced degradation under UV exposure [13]–[15], have weak mechanical strength [16], [17], and demonstrate tendency to suffer from biodegradation [18], [19].

Carbon-based sensors show promise in addressing the shortcomings of metal oxide and polymer based sensors [20]–[30]. Such sensors includes carbon nanotube (CNT) based sensors [20], [22], [31], [32], exfoliated graphene or reduced graphene oxide (rGO) based films [21], [26], polymer-graphene composite films [27], [29], [30], [33], and graphene/multilayer-

Manuscript received: 18 October 2018; revised: 6 February 2019; accepted: 1 March 2019. Date of publication: XX March 2019; date of current version: XX March 2019 This work is supported by the Faculty of Engineering and Physical Sciences at the University of Southampton, and the Malaysian Ministry of Education for the MyBRAIN15 MyPhD scholarship and research grant FRGS/2/2014/TK03/USMC/02/1.

T.Y. Ling is with the School of Electronics and Computer Science in University of Southampton, University Road, SO17 1BJ, Southampton, UK, and School of Engineering, University of Southampton Malaysia, Persiaran Canselor, Kota Ilmu @ Educity, 79200 Iskandar Puteri, Johor, Malaysia. (e-mail: ivan.ling@soton.ac.uk)

S.H. Pu is with the School of Engineering, University of Southampton Malaysia, Persiaran Canselor, Kota Ilmu @ Educity, 79200 Iskandar Puteri, Johor, Malaysia. (e-mail: suanhui.pu@soton.ac.uk)

S.J.Fishlock is with Nanotechnology and Integrated Bioengineering Center, University of Ulster, BT37 0QB, Newtownabbey, UK. (e-mail: s.fishlock@ulster.ac.uk)

Y.Han is with Department of Physics, University of Warwick, Coventry, West Midlands, CV4 7AL, UK. (yisong.han@warwick.ac.uk)

J.D. Reynolds is with the School of Electronics and Computer Science, University of Southampton UK (e-mail: J.D.Reynolds@soton.ac.uk)

J.W. McBride is with the School of Engineering, University of Southampton, UK. (j.w.mcbride@soton.ac.uk)

Harold M.H. Chong is with the School of Electronics and Computer Science, University of Southampton, UK. (hmhc@ecs.soton.ac.uk)

graphene/graphite films deposited using chemical vapour deposition (CVD) [24], [28], [34]. Carbon films with high sp^2 bonds (CNT, graphene, graphite) are known to be stable when exposed to environmental factors, such as weak acids and UV [35][36].

Amongst these techniques, CVD based carbon materials shows the most promise as it allows for controllable large area growth of carbon films. However, CVD grown carbon films, such as CVD graphene or CVD graphite has higher grain boundary (GB) concentration when compared to mechanically exfoliated graphene or highly ordered pyrolytic graphite (HOPG), which leads to degradation in its electron transport properties. However, work done by [37], [38] shows that such defects are actually crucial for carbon-based sensors, as they act as adsorption sites for the analytes. Several research groups published works on gas sensors based on nanocrystalline graphene with defects [39]–[42] synthesized using different methods. The feasibility of using nanocrystalline graphene field-effect transistors (FET) for humidity sensing was demonstrated by [25]. Nonetheless, there is a lack of literature on nanocrystalline graphite as humidity sensors, and we demonstrate that like nanocrystalline graphene, thicker nanocrystalline graphite (NCG) has the potential for robust humidity sensing applications. Recently, NCG grown directly on insulating substrate without the need for metal catalysts was demonstrated. The film has great potential to be used as a humidity sensor in dynamic environments due to its superior mechanical and chemical stability [39], [40], [43]–[46]. The high defect density of the film contributes both to its mechanical stability and its sensing ability.

In this work, we report for the first time, the use of nanocrystalline graphite in a humidity sensing application. We used catalyst-free plasma-enhanced CVD (PECVD) to deposit NCG directly onto silicon dioxide substrates, as resistive humidity sensors. The NCG used here is a thicker variant of the nanocrystalline graphene films reported in [47], and similar to the NCG films reported in [46], [48]. The films are mechanically stable, are suitable for use in harsh environments, and have great mechanical wear resistance [48]. Using this technology, nanocrystalline graphite films with different film morphologies can be deposited by tuning the deposition parameters [49], [50]. Our experiment shows that this device has the potential to perform well as a real-time resistive humidity sensor for harsh environments.

II. Materials and Methods

A. NCG Fabrication

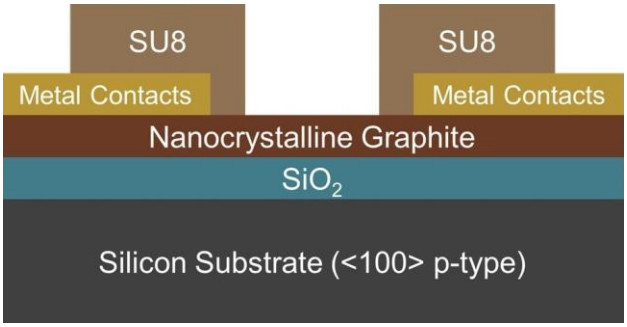

Fig. 1. Cross-sectional view of NCG sensor

The NCG films were grown directly onto a silicon dioxide (SiO2) layer with an average thickness of 460 nm which acts as a dielectric insulator to isolate the conductive NCG thin film from the underlying p-type Si substrate. Fig. 1 shows the cross-sectional view of the device fabricated. The SiO_2 layer was grown by wet thermal oxidation. The thickness profile was measured by ellipsometry (J.A. Woolham M2000 ellipsometer).

NCG deposition was carried out using PECVD at 850 ^oC under a constant flow of methane (CH_4) and hydrogen (H_2) in an Oxford Instruments Nanofab 1000 Agile PECVD Chamber at 100 W RF power. The film thickness was varied by changing the deposition time and measured by ellipsometry (J.A. Woolham M2000 ellipsometer), while the length and width profile are patterned using O_2 reactive ion etching (RIE). Metal contact pads, consisting of 20 nm of titanium and 400 nm of aluminum was deposited directly onto the NCG surface via electron beam evaporation using a Leybold BAK 600 E-beam Evaporator. To isolate the metal tracks on the chips from the analyte, 2.4 µm of SU8 was deposited using the spin-on process and patterned with standard photolithography. The SU8 was then cured at 200 ^oC to form a permanent protective layer.

B. Material Characterization

The NCG films were characterized by Raman spectroscopy, using the Renishaw inVia Raman Spectrometer with a 650 nm laser at a single spot with a spot size of about 1 µm. The Raman spectroscopy was performed at room temperature, and the laser power was kept constant at 5mW. The resultant spectra were comparable to those reported by [47], [48] for verification.

To further study the conductivity and the surface morphology of the thin film, a VEECO Multimode scanning probe microscope (SPM) was used. The SPM was configured as a tapping mode atomic force microscope (AFM) to measure the surface properties of the film using a standard n-doped Si tip. The scanning was done at 1 Hz and 512 lines, and the phase shift between the AFM tip and the driving oscillator was extracted. The phase image was used to resolve the different material phases instead of surface roughness.

Images of the film were also taken using a transmission electron microscope (TEM). The sample used for the TEM was taken from a different batch of wafers fabricated with the same process at a deposition temperature of 750^oC as it is a destructive characterization process. The similarity in the Raman spectrum of the samples was compared and verified to

This article has been accepted for publication in a future issue of this journal, but has not been fully edited. Content may change prior to final publication. Citation information: DOI 10.1109/JSEN.2019.2905719, IEEE Sensors Journal

establish the legitimacy of using samples from a different batch in the TEM characterization. The TEM samples were prepared using mechanical exfoliation into ethanol, sonicated for 10 minutes, and micropipetted into a copper supported holey carbon grid (Agar Scientific Holey Carbon Film on 300 mesh cu). HRTEM (JEOL JEM-2100F) was used for imaging at 200keV excitation. The selected area electron diffraction (SAED) image of the NCG was also taken to verify the nanocrystallinity of the film.

C. Response measurement

The fabricated chip (1cm × 1cm) was diced and assembled onto a PCB, the naming convention used, and the geometrical dimensions of the devices are summarized in Table 1. While images of the devices taken on an optical microscope were shown in Fig. 4. The chip was connected to the PCB through aluminum wire bonding (Fig. 3). The gas sensor PCB was then assembled onto the gas sensing rig via pin headers. The experiment was divided into 3 sets, which aims to test the effect of the device's width, thickness and exposed edge on the overall sensing performance of the sensor. For each set of experiments, different devices were used.

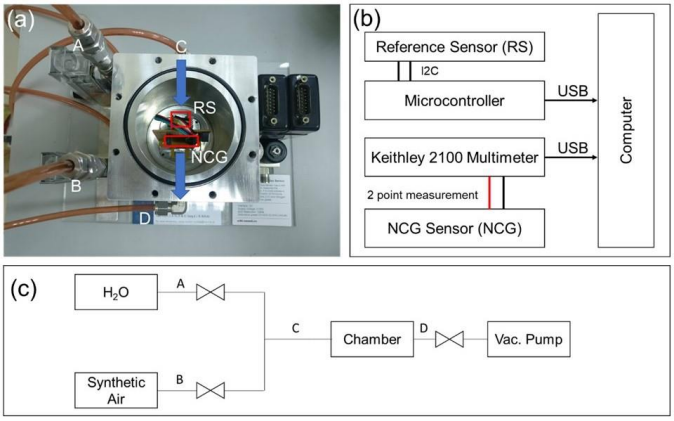

Fig. 2. (a) Humidity testing setup. Blue arrows on the picture show the direction of gas flow in the chamber. The cover of the chamber was removed for clarity. (b) electrical connection of the setup, (c) block diagram of the humidity test system

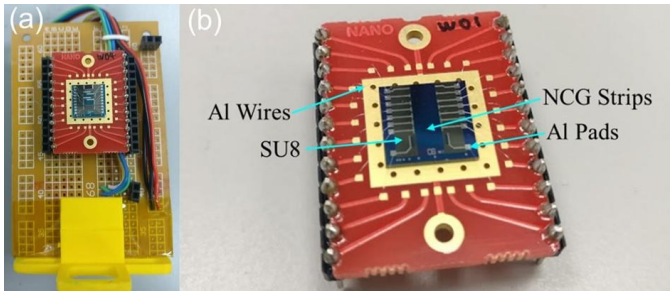

Fig. 3. (a) wire bonded chip attached on the testing rig. (b) close-up image of the wire-bonded chip.

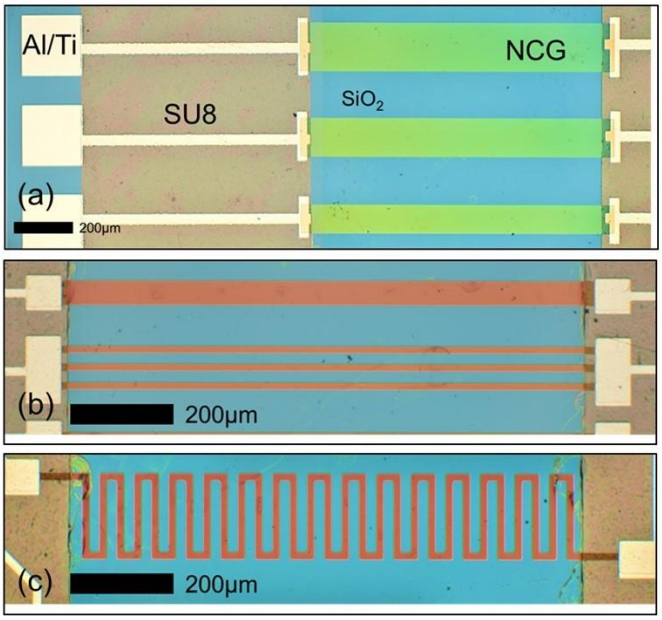

Fig. 4. (a) Optical microscope image of the strips used for testing. Device shown here are 300_3_30_Str (Bottom), 400_3_30_Str (Middle, Unused) and 500_3_30_Str (Top), (b) Single and arrayed NCG Strips 150_3_300_Str (Top) and 150_3_300_Arr (Bottom), (c) Optical Microscope image of 10_20_300_Mdr : Meandered strips

The sensors were tested in an environmental chamber fitted with a commercial Bosch Sensortec BME280 temperature, pressure and humidity sensor. The relative humidity of the gas chamber was increased by introducing water vapour through a commercial ultrasonic humidifier filled with deionized water (refer to Fig. 2). The term 'relative humidity', often used in literature, refers to the ratio between the partial pressure of water vapor in the air and the equilibrium vapor pressure of water on top of a flat surface of a body of water at a given temperature. At the beginning of each measurement cycle, the humidity of the chamber was lowered to 40% RH using 20 g of silica gel (Hannschweiller Chemicals GmbH) as the desiccant.

TABLE I
DESCRIPTION OF DEVICES

Device ID	Width (μm)	Length (mm)	Thickness (nm)	Description
100_3_30_Str	100	3	30	Straight strips
300_3_30_Str	300	3	30	Straight strips
500_3_30_Str	500	3	30	Straight strips
10_20_30_Mdr	10	20	30	Meandered strips
10_20_300_Mdr	10	20	300	Meandered strips
150_3_300_Str	150	3	300	Straight strips
150_3_300_Arr	50×3	3	300	Array strips with the same top surface area.

This article has been accepted for publication in a future issue of this journal, but has not been fully edited. Content may change prior to final publication. Citation information: DOI 10.1109/JSEN.2019.2905719, IEEE Sensors Journal

Synthetic air (Calgaz, 20% O_2 in N_2 balance, Relative humidity < 25% RH) was used to remove excess moisture if necessary.

Humidity was increased by feeding water vapour created from the humidifier into the chamber for 3 seconds. After that, the chamber was sealed, and resistance was logged every 2 seconds using a Keithley 2100 high precision multimeter. A 30-minute delay was introduced after each humidity pulse for sensor signal stabilization. The resultant response of the sensor was shown in Fig. 5.

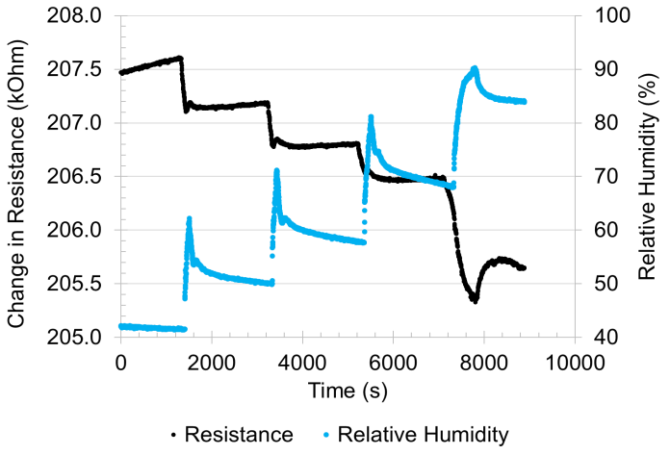

Fig. 5. Response of sensor (10_20_300_Mdr) to different values of relative humidity in steps

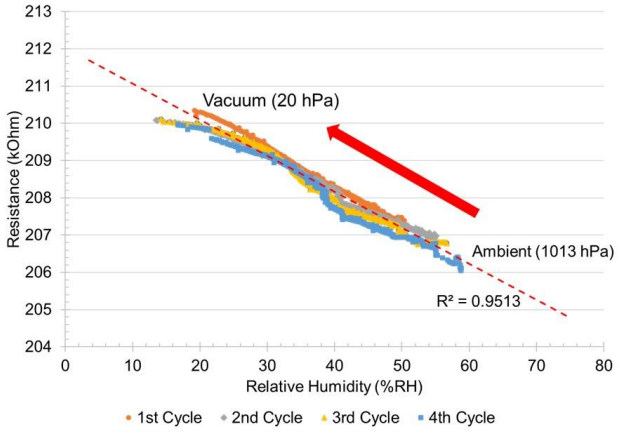

Fig. 6. Resistance as a function of relative humidity, taken as an aggregate of 4 vacuum-ambient measurement cycles from 10_20_300_Mdr

An additional measurement cycle was carried out using a vacuum pump on a sealed chamber to establish the relationship between the sensor's resistance at lower relative humidity values. The chamber was pumped down from 1013 hPa (1 atm) to 20 hPa (0.0197 atm) and the humidity was increased by introducing atmospheric air. Fig. 6 shows the measurement results obtained, which fits linearly with the results obtained for higher relative humidity values. Correlational studies were carried out to determine the correlation between humidity, pressure and resistance. The results show little correlation between pressure and resistance. Any apparent sensitivity between pressure and the resistance arises due to the correlation between pressure and humidity. In the absence of water vapour, the strip shows no significant response to changing air pressure.

The sensor shows high repeatability across 4 measurement cycles, with an R^2 value of 0.95. To verify that the effect of measurement is from the NCG film, and not the metal contacts, a set of NCG films with similar geometrical dimensions were fabricated and covered entirely with SU8. Tests on these devices show no response to change in humidity.

III. Results and Discussion

A. Film characteristics

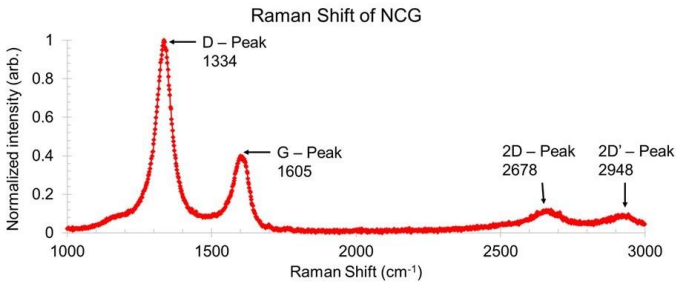

Fig. 7. Raman spectrum of the PECVD grown NCG of 200nm thickness

The Raman spectrum of the film (Fig. 7) exhibits clear D, G, and 2D peaks. The high D-peak in the spectrum is characteristic of defective graphene sheets. The high D-peak intensity also indicates a higher number of crystalline defects (line or point defects) in the underlying graphene structure in each layer [51]. The G-peak represents the radial breathing mode of the sp^2 carbon in the aromatic ring structures found in graphene/graphite crystals. The D/G intensity ratio of about 2 strongly suggests the presence of NCG in the thin film based on the three stage model of increasing disorder in carbon films proposed by [51], which indicates a high distribution of crystalline defects and edge defects, with the presence of small pockets with aromatic sp^2 rings, suggesting a film with graphite/graphite nanocrystals separated by amorphous carbon grain boundaries. The spectrum was similar to other reported instances of NCG by other research groups [39], [40], [52].

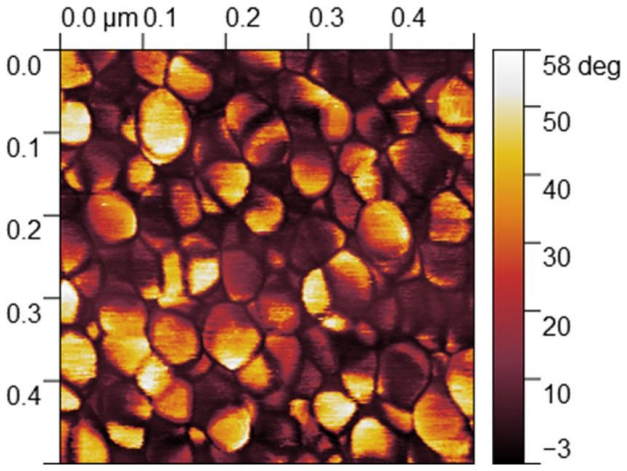

Fig. 8. AFM phase image showing clear granular characteristic and grain boundaries

This article has been accepted for publication in a future issue of this journal, but has not been fully edited. Content may change prior to final publication. Citation information: DOI 10.1109/JSEN.2019.2905719, IEEE Sensors Journal

The AFM image (Fig. 8) shows the clear granular structure of the deposited NCG. The bright and dark areas of the film represent the phase shift between the oscillating cantilever of the AFM and the reference oscillator. Since the phase shift of the cantilever is sensitive to the surface stiffness and adhesion properties [53], the phase image clearly shows the presence of two different material on the film. The AFM image shows evidence that the film is made up of crystalline grains in random orientations surrounded by amorphous carbons in the grain boundary which we further investigate using transmission electron microscope (TEM) as shown in Fig. 9(a). The TEM image shows grains of graphite nano-crystals dispersed randomly in a matrix of amorphous carbon. In some areas, the grains appear to form by multiple crystallites.

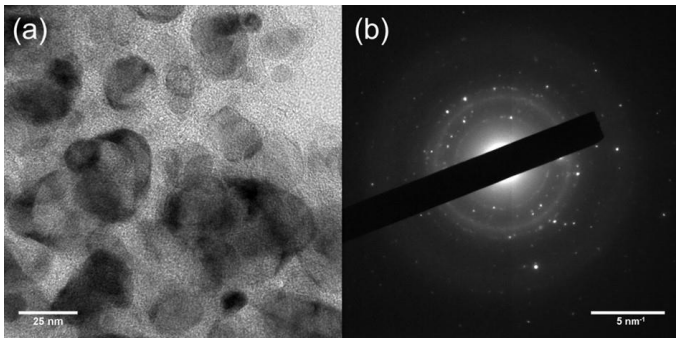

Fig. 9. (a) TEM image showing the granular structure of the NCG film (b) SAED Image of NCG film

The selected-area electron diffraction (SAED) image of the NCG film (Fig. 9(b)) shows a mixture of spots and diffuse rings. The brightness of the spots could be attributed to the size of crystalline domains found on the sample, while the position of the spots on the SAED indicates the crystal orientation. Since the nanocrystals are oriented randomly, there is no clear geometrical pattern, which would be indicative of a crystalline structure, but rather a series of bright spots disperse randomly in a ring. As the crystals get smaller and more amorphous, the spots grow dimmer and are dispersed more randomly around the ring. Therefore, the presence of diffused patterns can be attributed to the amorphous regions in the film [54].

B. Humidity response of NCG films

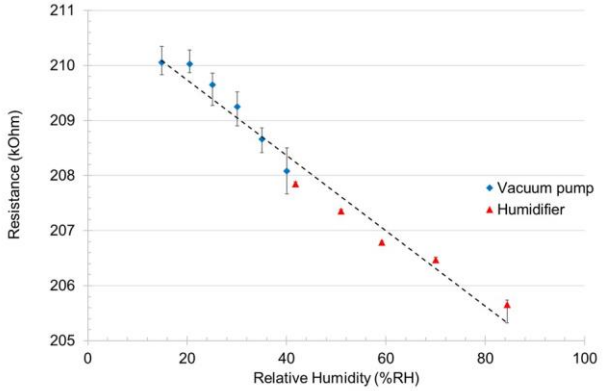

Fig. 10. Resistance of NCG meandering strip (10_20_300_Mdr) as a function of humidity

Fig. 10 shows the average resistance measured of the NCG sensor recorded using different methods. For sub-room humidity level measurements, the statistical values are derived from Fig. 6, while for higher humidity readings, the values are taken using values from Fig. 5.

The overall trend shows a decrease in resistance, which suggests the formation of shunt paths across grain boundaries in the strip. As graphene crystals are highly conductive, the film's resistance is dominated by the grain boundaries and defects. The predicted baseline humidity at 0% RH, R_0, is calculated for each fabricated device by linear extrapolation of the best fit line. The coefficient of determination of the best fit line, the predicted R_0, the sensitivity of the sensor, and the magnitude of resistance change are tabulated in Table 2.

Due to the different ways of calculating the figure of merits in literature, the figure of merits from each literature was converted to the following standardized form:

$$S = \left| \left(\frac{\Delta R}{R_0 \times RH} \right) \times 100\% \right|$$

Whenever possible, the resistance measured is used, in other cases, where the resistance values are unobtainable, we used the reported parameter for the response. It is also worth noting that the percentage change reported here are taken as absolute values. Our film is comparable in performance to that of graphene oxide films and superior to carbon nanotubes. We would also like to mention that work done by [24] has shown that multilayer graphene and graphene has alternating resistance change due to the competing effects of charge transfer and protonic conduction. Sensors which use bilayer [21] and CVD graphene [23], have higher sensitivity, but require a more complicated synthesis process, where the graphene needs to be grown on a metal catalyst layer before being transferred to the desired substrate.

From the time-domain signal of the sensor, sensor responded faster than the reference sensor (>2s). Our tests show that the main limitation for the sensor's response was the ADC integration time of the multimeter, which was 20ms. A slight hysteresis of 5%RH was observed at high humidity reading (> 80% RH) due to condensation of water on the sensor surface.

TABLE II
SUMMARY OF DEVICE TESTED

Device ID	Slope of best fit line ($\Delta R/R_0$/%RH ×100%)	Coefficient of determination, R^2	R_0 (MOhm)	ΔR_{max} (kOhm)
100_3_30_Str	0.0172	0.966	0.1014	-1.743
300_3_30_Str	0.0137	0.910	0.0335	-0.439
500_3_30_Str	0.0126	0.984	0.0203	-0.286
10_20_30_Mdr	0.0290	0.961	1.0160	-44.751
10_20_300_Mdr	0.0334	0.951	0.2111	-6.892
150_3_300_Str	0.0234	0.953	0.0144	-0.329
150_3_300_Arr	0.0260	0.955	0.0147	-0.374

This article has been accepted for publication in a future issue of this journal, but has not been fully edited. Content may change prior to final publication. Citation information: DOI 10.1109/JSEN.2019.2905719, IEEE Sensors Journal

TABLE III
COMPARISON WITH OTHER PUBLISHED WORKS

Sensing Material	Method of detection	Figure of Merit S = (ΔR/R/%RH)×100% unless stated otherwise	Tested Range	Ref
Graphene oxide and amine modified graphene oxide	Capacitance and conductance	S_{max} = 9.67% (capacitance) S_{max} = 0.0463% (conductance)	5% RH – 95% RH	[21]
CVD Graphene	Resistance	S = 0.31%	1% RH – 96% RH	[23]
Multilayer graphene (MLG) and Graphene	Resistance	S = 0.1% - 0.17% Response is non-linear, reported as [(ΔR/Rx100%)/%RH] × 100% = 10% Work shows various strip with alternating resistance change to explore the origins of such change.	15% RH – 80% RH	[24]
Bilayer Graphene	Resistance	S = 0.181% Sensitivity calculated in terms of current instead of resistance	35% RH – 98% RH	[28]
Black phosphorus (BP) – Graphene hybrid	Resistance	S = 0.62% (as fabricated) S < 0.14% (after 4 weeks)	15% RH – 70% RH	[30]
Carbon nanotube on cellulose paper	Resistance	S = 6% Sensitivity calculated in terms of conductance	10% RH – 70% RH After 70% sensor loses linearity due to degradation of cellulose paper.	[20]
PDDA/Reduced graphene oxide (RGO)	Resistance	S = 8.69–37.43%	11% RH - 97% RH	[27]
Multiwall carbon nanotube/polyimide composite	Resistance	S = 0.0047%	10% RH – 95% RH	[22]
Nanocrystalline Graphite	Resistance	S = 0.0334%	15% RH – 85% RH	[This Work]

The hysteresis was not observed when the humidity was cycled quickly without any condensation using vacuum pump.

In Fig. 11, we show that as the widths of the devices are increased, the gradient of the resistance change to relative humidity slope decreases gradually. In usual sensors, gas or moisture adsorbed onto the surface of the sensors contribute to the change in resistance, hence, increasing the total surface area should increase the percentage of change in resistance. However, in the case of NCG, the effect seems to be anisotropic. An increase in the width of the strips appears to cause a decrease in the percentage of response. A possible cause is that majority of the moisture are adsorbed on the side walls of the device which has a higher edge defect density. There is also a possibility that the moisture adsorbs more at the NCG – SiO_2 interface due to capillary effect. This is consistent with the effects of ionic humidity detection reported in various ceramic sensors [6], [55].

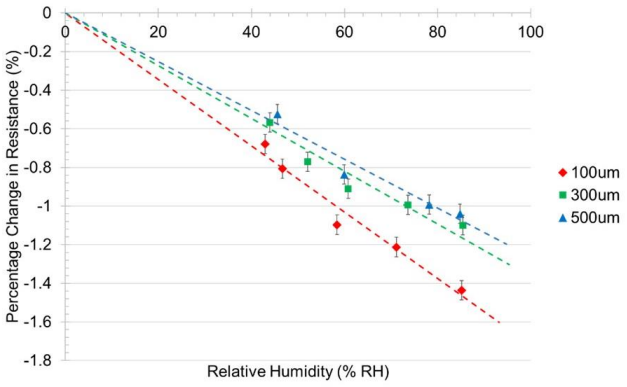

Fig. 11. Percentage of change in resistance of the sensor as a function of relative humidity for devices with different widths but same thickness and length. Thickness = 30 nm, length = 3 mm

This article has been accepted for publication in a future issue of this journal, but has not been fully edited. Content may change prior to final publication. Citation information: DOI 10.1109/JSEN.2019.2905719, IEEE Sensors Journal

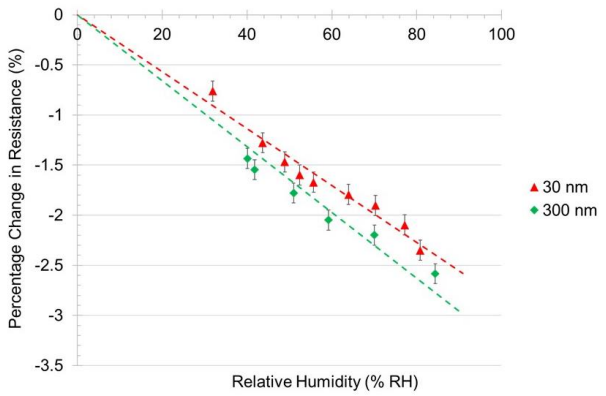

Fig. 12. Percentage of change in resistance in strips as a function of relative humidity for devices with different thickness but same width and length. Width = 10 µm, length = 20 mm (Meandered strips)

To verify the hypothesis, a much narrower and longer strip was used. Two devices with the same width and length, but a different thickness, were tested (refer to Fig. 4(c)), and the results are shown in Fig. 13. For the same top surface exposed, the thicker strip experiences a slightly higher percentage change in resistance. Note that these devices are meandered strips, hence, the higher percentage of change in comparison to the straight strips can be attributed to the longer and narrower structure of the device.

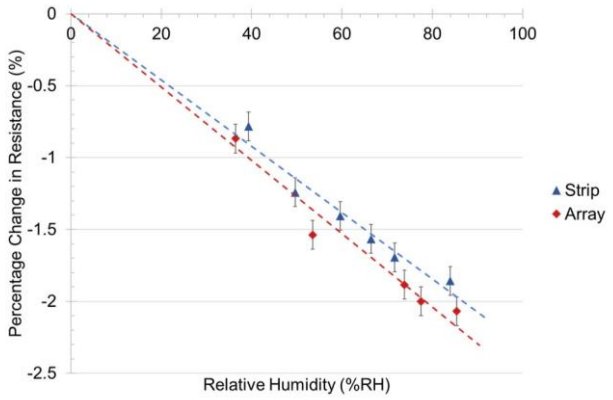

Fig. 13. Percentage of change in conductance in strips as a function of relative humidity for devices with the same total top surface area, but different amount of side walls exposed. Thickness = 300 nm, length = 3 mm, width = 150 µm (Strip) & 50µm x 3 (Arrays)

To vary the number of sidewalls exposed, one device consists of a 150 µm NCG strip, while the other is an array of 3x50µm NCG array (refer Fig. 4(b)). Both devices have the same length and thickness. shows the device with more side walls exposed has a slightly higher slope in the percentage of resistance change to relative humidity curve, but the overall difference in the percentage of change is not very significant (Refer to Table 2 for sensitivity value). It is possible that for wider and shorter strips, the effects of water adsorption on the surface is dominant. However, as the strips become narrower and longer, the effects of capillary adsorption become more dominant.

C. *Sensing mechanism*

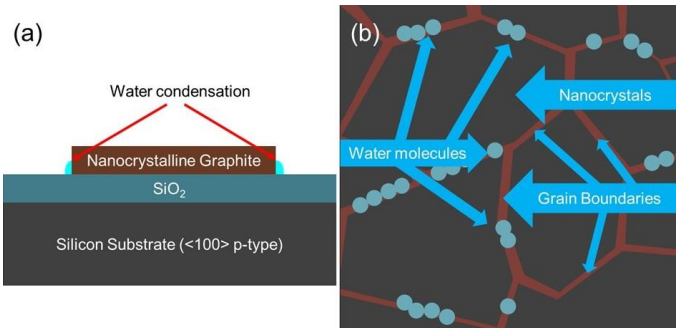

Fig. 14. (a) Illustration of possible condensation point between side-wall and substrate due to capillary effect (b) Illustration of water molecules forming a conductive pathway on the film surface.

From the results, it appears that the amount of side surface area exposed affects the sensitivity of the film. In an extremely thin film with a large surface area of the same material, the dominant sensing mechanism appear to be charge transfer, as observed in previous studies done by [24], [28]. However, as the size of the NCG sensors is being scaled down, the effects of surface charge transfer diminishes. As the width of the devices tends towards the micrometre scale, conductive pathways formed due to adsorbed water molecules become significant. At the same time, due to capillary effect between the side walls of the strip and the substrate, water molecules may adsorb more readily at the sides of the film, hence causing a further decrease in resistance. For a change in conductivity to occur, the adsorbed water molecule need not form a continuous film over the whole surface of the sensor. If the physisorbed water molecules are close together, they readily form a protonic conduction chains via the Grotthuss mechanism (refer Fig. 14) [18,34] In such a chain, conduction will be carried out through proton tunneling from one water molecule to the other ($H^+ + H_2O \rightarrow H_3O^+$, and subsequently $H_3O^+ + H_2O \rightarrow H_2O + H_3O^+$ until the end of the conduction chain). Due to the presence of highly conductive graphite crystals and highly resistive amorphous carbon in the film, localized 'pool' of the adsorbed water molecule can readily form a shunt between successive graphitic crystals, causing a noticeable drop in resistance.

IV. Conclusion

A humidity sensor based on NCG was fabricated using catalyst-free PECVD onto SiO_2 substrate. The performance of the sensor with different geometrical dimension was evaluated from 15% RH to 85% RH. It is believed that the Grotthuss mechanism plays an important role in modulating the resistance of the resistive strips. Shunt created by protonic conduction due to adsorption of water molecule dominates the effect of charge transfer in thicker, but narrower films, where the edge effect dominates. The film shows great potential to be used in applications where polymer and metal oxide sensors are unsuitable, such as wearable electronics where the robustness of the sensor is a priority.

REFERENCES

[1] A. E. Dessler and S. C. Sherwood, "Atmospheric science: A matter of humidity," *Science (80).*, vol. 323, no. 5917, pp. 1020–1021, 2009.

[2] C. C. Hu and H. L. Li, "Indoor thermal comfort controls optimized by deducing rules," *Int. Conf. Adv. Commun. Technol. ICACT*, vol. 2016–March, pp. 26–30, 2016.

[3] G. Mauris and L. Foulloy, "A fuzzy symbolic approach to formalize sensory measurements: An application to a comfort sensor," *IEEE Trans. Instrum. Meas.*, vol. 51, no. 4, pp. 712–715, 2002.

[4] L. Jingjie, Y. Dongmei, Z. Ruiyi, and Z. Hui, "A humidity control system based on T&H-decoupling and PID self-tuning fuzzy algorithm," *2017 13th IEEE Int. Conf. Electron. Meas. Instruments*, pp. 16–21, 2017.

[5] L. Zipser, H. Franke, and W. D. Bretschneider, "Robust acoustic humidity sensor for industrial drying," *Proc. IEEE Sensors 2004, Vols 1-3*, p. 107–110, 1596, 2004.

[6] T. Seiyama, N. Yamazoe, and H. Arai, "Humidity sensors*," vol. 4, pp. 86–96, 1983.

[7] W. Qu and J.-U. Meyer, "A novel thick-film ceramic humidity sensor," *Sensors Actuators B Chem.*, vol. 40, no. 2–3, pp. 175–182, 1997.

[8] M. Ahmadipour, M. F. Ain, and Z. A. Ahmad, "Fabrication of resistance type humidity sensor based on CaCu3Ti4O12 thick film," *Meas. J. Int. Meas. Confed.*, vol. 94, pp. 902–908, 2016.

[9] J. J. Steele, M. T. Taschuk, and M. J. Brett, "Nanostructured metal oxide thin films for humidity sensors," *IEEE Sens. J.*, vol. 8, no. 8, pp. 1422–1429, 2008.

[10] M. Packirisamy, I. Stiharu, X. Li, and G. Rinaldi, "A polyimide based resistive humidity sensor," *Sens. Rev.*, vol. 25, no. 4, pp. 271–276, 2005.

[11] Z.-T. Zhu, J. T. Mason, R. Dieckmann, and G. G. Malliaras, "Humidity sensors based on pentacene thin-film transistors," *Appl Phys Lett*, vol. 81, no. May 2014, pp. 4643–4645, 2002.

[12] C.-Y. Lee and G.-B. Lee, "Micromachine-based humidity sensors with integrated temperature sensors for signal drift compensation," *J. Micromechanics Microengineering*, vol. 13, no. 5, p. 620, 2003.

[13] N. Nagai, T. Matsunobe, and T. Imai, "Infrared analysis of depth profiles in UV-photochemical degradation of polymers," *Polym. Degrad. Stab.*, vol. 88, no. 2, pp. 224–233, 2005.

[14] A. Andrady, H. Hamid, and A. Torikai, "Effects of solar UV and climate change on materials," *Photochem. Photobiol. Sci.*, vol. 10, no. 292, 2011.

[15] H. Zhao and R. K. Y. Li, "A study on the photo-degradation of zinc oxide (ZnO) filled polypropylene nanocomposites," *Polymer (Guildf).*, vol. 47, no. 9, pp. 3207–3217, 2006.

[16] A. F. Diaz and B. Hall, "Mechanical Properties of Electrochemically Prepared Polypyrrole Films," *IBM J. Res. Dev.*, vol. 27, no. 4, pp. 342–347, 1983.

[17] R. A. Green, N. H. Lovell, G. G. Wallace, and L. A. Poole-Warren, "Conducting polymers for neural interfaces: Challenges in developing an effective long-term implant," *Biomaterials*, vol. 29, no. 24–25, pp. 3393–3399, 2008.

[18] J. M. Restrepo-Flórez, A. Bassi, and M. R. Thompson, "Microbial degradation and deterioration of polyethylene - A review," *Int. Biodeterior. Biodegrad.*, vol. 88, pp. 83–90, 2014.

[19] B. Nowak, J. Pajak, M. Drozd-Bratkowicz, and G. Rymarz, "Microorganisms participating in the biodegradation of modified polyethylene films in different soils under laboratory conditions," *Int. Biodeterior. Biodegrad.*, vol. 65, no. 6, pp. 757–767, 2011.

[20] J. W. Han, J. L. Beomseok Kim, and M. Meyyappan, "Carbon Nanotube Based Humidity Sensor on Cellulose Paper," *J. od Phys. Chem. C*, no. OCTOBER 2012, pp. 22094–22097, 2012.

[21] S. W. Lee, B. Il Choi, J. C. Kim, S. B. Woo, Y. G. Kim, S. Kwon, J. Yoo, and Y. S. Seo, "Sorption/desorption hysteresis of thin-film humidity sensors based on graphene oxide and its derivative," *Sensors Actuators, B Chem.*, vol. 237, pp. 575–580, 2016.

[22] K. P. Yoo, L. T. Lim, N. K. Min, M. J. Lee, C. J. Lee, and C. W. Park, "Novel resistive-type humidity sensor based on multiwall carbon nanotube/polyimide composite films," *Sensors Actuators, B Chem.*, vol. 145, no. 1, pp. 120–125, 2010.

[23] A. D. Smith, K. Elgammal, F. Niklaus, A. Delin, A. C. Fischer, S. Vaziri, F. Forsberg, M. Råsander, H. Hugosson, L. Bergqvist, S. Schröder, and S. Kataria, "Nanoscale and direct electrical readout †," pp. 19099–19109, 2015.

[24] V. I. Popov, D. V Nikolaev, V. B. Timofeev, S. A. Smagulova, and I. V Antonova, "Graphene-based humidity sensors : the origin of alternating resistance change," 2017.

[25] D. Noll, U. Schwalke, and T. U. Darmstadt, "Feasibility study of in-situ grown nanocrystalline graphene for humidity sensing," pp. 2–5, 2017.

[26] S. Borini, R. White, D. Wei, M. Astley, S. Haque, E. Spigone, N. Harris, J. Kivioja, and T. Ryhänen, "Ultrafast graphene oxide humidity sensors," *ACS Nano*, vol. 7, no. 12, pp. 11166–11173, 2013.

[27] D. Zhang, J. Tong, and B. Xia, "Humidity-sensing properties of chemically reduced graphene oxide/polymer nanocomposite film sensor based on layer-by-layer nano self-assembly," *Sensors Actuators, B Chem.*, vol. 197, pp. 66–72, 2014.

[28] M.C. Chen, C.L. Hsu, and T.J. Hsueh, "Fabrication of Humidity Sensor Based on Bilayer Graphene," *IEEE Electron Device Lett.*, vol. 35, no. 5, pp. 590–592, 2014.

[29] Z. Yuan, H. Tai, Z. Ye, C. Liu, G. Xie, X. Du, and Y. Jiang, "Novel highly sensitive QCM humidity sensor with low hysteresis based on graphene oxide (GO)/poly(ethyleneimine) layered film," *Sensors Actuators, B Chem.*, vol. 234, pp. 145–154, 2016.

[30] D. T. Phan, I. Park, A. R. Park, C. M. Park, and K. J. Jeon, "Black P/graphene hybrid: A fast response humidity sensor with good reversibility and stability," *Sci. Rep.*, vol. 7, no. 1, pp. 1–7, 2017.

[31] Y. Zhang, K. Yu, R. Xu, D. Jiang, L. Luo, and Z. Zhu, "Quartz crystal microbalance coated with carbon nanotube films used as humidity sensor," *Sensors Actuators, A Phys.*, vol. 120, no. 1, pp. 142–146, 2005.

[32] J. T. W. Yeow and J. P. M. She, "Carbon nanotube-enhanced capillary condensation for a capacitive humidity sensor," *Nanotechnology*, vol. 17, no. 21, pp. 5441–5448, 2006.

[33] W. De Lin, H. M. Chang, and R. J. Wu, "Applied novel sensing material graphene/polypyrrole for humidity sensor," *Sensors Actuators, B Chem.*, vol. 181, pp. 326–331, 2013.

[34] A. D. Smith, K. Elgammal, F. Niklaus, A. Delin, A. C. Fischer, S. Vaziri, F. Forsberg, M. Rasander, H. Hugosson, L. Bergqvist, S. Schröder, S. Kataria, M. Ostling, and M. C. Lemme, "Resistive graphene humidity sensors with rapid and direct electrical readout," *Nanoscale*, vol. 7, no. 45, pp. 19099–19109, 2015.

[35] F. Hine, *Electrode Processes and Electrochemical Engineering*. Plenum Press, 1985.

[36] A. Ghasemi-Kahrizsangi, J. Neshati, H. Shariatpanahi, and E. Akbarinezhad, "Improving the UV degradation resistance of epoxy coatings using modified carbon black nanoparticles," *Prog. Org. Coatings*, vol. 85, pp. 199–207, 2015.

[37] F. Ricciardella, S. Vollebregt, T. Polichetti, M. Miscuglio, B. Alfano, M. L. Miglietta, E. Massera, G. Di Francia, and P. M. Sarro, "Effects of graphene defects on gas sensing properties towards NO_2 detection," *Nanoscale*, vol. 9, no. 18, pp. 6085–6093, 2017.

[38] S. S. Varghese, S. Lonkar, K. K. Singh, S. Swaminathan, and A. Abdala, "Recent advances in graphene based gas sensors," *Sensors Actuators, B Chem.*, vol. 218, pp. 160–183, 2015.

[39] M. V. S. Chandrashekhar, J. Lu, M. G. Spencer, M. Qazi, and G. Koley, "Large area nanocrystalline graphite films on SiC for gas sensing applications," *Proc. IEEE Sensors*, pp. 558–561, 2007.

[40] R. C. Mani, M. K. Sunkara, R. P. Baldwin, J. Gullapalli, J. A. Chaney, G. Bhimarasetti, J. M. Cowley, A. M. Rao, and K. Rao, "Nanocrystalline graphite for electrochemical sensing," *J. Electrochem. Soc.*, vol. 152, no. 4, pp. E154–E159, 2005.

[41] A. Serra, A. Buccolieri, E. Filippo, and D. Manno, "Nanographite assembled films for sensitive NO 2 detection," *Sensors Actuators, B Chem.*, vol. 161, no. 1, pp. 359–365, 2012.

[42] G. Lu, L. E. Ocola, and J. Chen, "Reduced graphene oxide for room-temperature gas sensors.," *Nanotechnology*, vol. 20, no. 44, p. 445502, 2009.

[43] S. Fishlock, H. Chong, J. Mcbride, S. O. Shea, and S. H. Pu, "Characterisation of nanographite for MEMS resonators Carbon materials for MEMS and NEMS," 2015.

[44] M. E. Schmidt, "Plasma enhanced chemical vapor deposition of nanocrystalline graphene and device fabrication development," 2012.

[45] J. Sun, M. E. Schmidt, M. Muruganathan, H. M. H. Chong, and H. Mizuta, "Large-scale nanoelectromechanical switches based on directly deposited nanocrystalline graphene on insulating substrates," *Nanoscale*, vol. 8, no. 12, pp. 6659–6665, 2016.

[46] S. J. Fishlock, S. J. O'Shea, J. W. McBride, H. M. H. Chong, and S. H. Pu, "Fabrication and characterisation of nanocrystalline graphite

MEMS resonators using a geometric design to control buckling," *J. Micromechanics Microengineering*, vol. 27, no. 9, 2017.

[47] M. E. Schmidt, C. Xu, M. Cooke, H. Mizuta, and H. M. H. Chong, "Metal-free plasma-enhanced chemical vapor deposition of large area nanocrystalline graphene," *Mater. Res. Express*, vol. 1, no. 2, p. 025031, 2014.

[48] S. Rana, J. D. Reynolds, T. Y. Ling, M. S. Shamsudin, S. H. Pu, H. M. H. Chong, and D. Pamunuwa, "Nano-crystalline graphite for reliability improvement in MEM relay contacts," *Carbon N. Y.*, vol. 133, pp. 193–199, 2018.

[49] L. Zhang, Z. Shi, Y. Wang, R. Yang, D. Shi, and G. Zhang, "Catalyst-free growth of nanographene films on various substrates," *Nano Res.*, vol. 4, no. 3, pp. 315–321, 2011.

[50] A. V. Tyurnina, K. Tsukagoshi, H. Hiura, and A. N. Obraztsov, "Structural and charge transport characteristics of graphene layers obtained from CVD thin film and bulk graphite materials," *Carbon N. Y.*, vol. 52, pp. 49–55, 2013.

[51] A. C. Ferrari and J. Robertson, "Raman spectroscopy of amorphous, nanostructured, diamond-like carbon, and nanodiamond.," *Philos. Trans. A. Math. Phys. Eng. Sci.*, vol. 362, no. 1824, pp. 2477–2512, 2004.

[52] S. K. Jerng, D. S. Yu, Y. S. Kim, J. Ryou, S. Hong, C. Kim, S. Yoon, D. K. Efetov, P. Kim, and S. H. Chun, "Nanocrystalline graphite growth on sapphire by carbon molecular beam epitaxy," *J. Phys. Chem. C*, vol. 115, no. 11, pp. 4491–4494, 2011.

[53] S. N. Magonov, V. Elings, and M. H. Whangbo, "Phase imaging and stiffness in tapping-mode atomic force microscopy," *Surface Science*, vol. 375, no. 2–3. 1997.

[54] N. J. Hargreaves and S. J. Cooper, "Nanographite Synthesized from Acidified Sucrose Microemulsions under Ambient Conditions," *Cryst. Growth Des.*, vol. 16, no. 6, pp. 3133–3142, 2016.

[55] E. Traversa, G. Gnappi, A. Montenero, and G. Gusmano, "Ceramic thin films by sol-gel processing as novel materials for integrated humidity sensors," *Sensors Actuators B Chem.*, vol. 31, no. 1–2, pp. 59–70, 1996.

[56] H. Farahani, R. Wagiran, and M. N. Hamidon, *Humidity sensors principle, mechanism, and fabrication technologies: A comprehensive review*, vol. 14, no. 5. 2014.